Selective Photooxidation of Methane to Methanol with Oxygen over Dual-Cocatalysts Modified Titanium Dioxide

Hui Song,[1,2] Xianguang Meng,[1,3] Shengyao Wang,[1,5*] Wei Zhou,[6] Shuang Song,[1] Tetsuya Kako,[1] Jinhua Ye[1,2,4*]*

[1]International Center for Materials Nanoarchitectonics (WPI-MANA), National Institute for Materials Science (NIMS), 1-1 Namiki, Tsukuba, Ibaraki 305-0044, Japan

[2]Graduate School of Chemical Sciences and Engineering, Hokkaido University, Sapporo 060-0814, Japan

[3]Hebei Provincial Laboratory of Inorganic Nonmetallic Materials, College of Materials Science and Engineering, North China University of Science and Technology, Tangshan 063210, P. R. China

[4]TJU-NIMS International Collaboration Laboratory, School of Material Science and Engineering, Tianjin University, Tianjin 300072, P. R. China

[5]College of Science, Huazhong Agricultural University, Wuhan 430070, P. R. China

[6]Department of Applied Physics, Tianjin Key Laboratory of Low Dimensional Materials Physics and Preparing Technology Faculty of Science, Tianjin University, Tianjin 300072, P. R. China

***Correspondence Authors**:

Jinhua.YE@nims.go.jp,

mengxg_materchem@163.com,

wangshengyao@mail.hzau.edu.cn

ABSTRACT

Direct and selective oxidation of CH_4 with dioxygen to methanol is a “dream reaction” in modern catalysis, yet remains a great challenge. Here, we report that TiO_2 loaded with dual-cocatalysts, i.e., nanometals and cobalt oxide (CoO_x) nanoclusters, is capable of selectively catalyzing CH_4 to CH_3OH at room temperature under photoexcitation using abundant and inexpensive O_2 as oxidant. The best activity for the formation of the primary products, CH_3OOH and CH_3OH, is up to 50.8 μmol for 2 h with 95% selectivity. Mechanistic studies elucidate that the superior activity and selectivity result from the synergistic effect of nanometals and CoO_x. Nanometals enhance CH_4 conversion by promoting the separation of photoexcited electron and the reduction of O_2. The CoO_x mediates a mild CH_4 oxidation process by suppressing the formation of highly oxidative $^{\bullet}OH$ radicals that can further oxidize CH_3OH to HCHO and CO_2, thereby preserving a high selectivity towards oxygenated products. This work provides a prototype in designing efficient photocatalysts for selective oxidation of CH_4 to CH_3OH with O_2 under mild conditions.

KEYWORDS: Methane oxidation, methanol, photocatalysis, titanium dioxide, dual-cocatalysts, nanometals, cobalt oxide.

Introduction

The high availability of methane (CH_4) from natural gas, shale gas, biogas and coalbed gas makes it a promising feedstock for the production of fuels and chemical commodities, such as methanol (CH_3OH). However, due to the high dissociation energy of first C-H bond in CH_4 (439 kJ mol^{-1}), direct activation of CH_4 remains a great challenge.[1,2] Industrially, the production of CH_3OH from CH_4 is an indirect process, involving the formation of syngas at high temperatures (>700 °C) by steam reforming and subsequent conversion of syngas to CH_3OH under high pressures.[3-5] Direct oxidation of CH_4 to CH_3OH is a promising alternative approach, due to the advantage of ideally avoiding the energy-intensive syngas process.[1] Recently, many impressive progresses for direct methane oxidation are achieved under mild conditions using heterogeneous catalysts such as Au-Pd colloids,[6] Cu or Fe-zeolites[7,8] and single Fe or Rh atoms catalysts,[9-11] in which methane can be selectively oxidized into methyl hydroperoxide (CH_3OOH, a liquid oxygenate that can be further converted into CH_3OH[6]) and/or CH_3OH. Although numerous catalysts and catalytic systems have been developed, thermocatalytic processes for direct oxidation of CH_4 to CH_3OH are currently subject to practical and economic constraints, such as high reaction temperatures and costly oxidants (H_2O_2 and N_2O).[1,5]

Photocatalysis using photoenergy and semiconductor could drive many tough reactions such as water splitting, N_2 fixation and CO_2 reduction at ambient temperatures.[12-17] Recently, photocatalytic CH_4 conversion has attracted increasing interest because it can be operated under mild reaction conditions.[17] Gas phase products such as CO_2, CO, C_2H_6 and H_2 are the main products in photocatalytic reaction systems, but most of them are limited by obvious overoxidation poor sustainability and low efficiency.[18-24] TiO_2-supported Fe species has recently been reported

as an efficient catalyst for photocatalytic CH_4 oxidation to CH_3OH in water using H_2O_2 as the oxidant at ambient conditions.[25] It is worthy of developing photocatalytic systems for room-temperature CH_4 conversion to CH_3OH using the abundant and inexpensive O_2 as the oxidant.[1,3,26] However, in gas phase reaction systems, the polar CH_3OH molecule could be easily adsorbed on the catalysts surface, thus resulting in the overoxidation of oxygenated product into CO_2 as the more thermodynamically stable product.[1] Our group have recently shown that nanometals-loaded ZnO are able to photocatalytically oxidize CH_4 to liquid oxygenates including CH_3OH and formaldehyde (HCHO) with O_2 in water.[27] Nonetheless, the selectivity towards CH_3OH is still unsatisfied (<70%) and the performance of ZnO is hampered by its stability. TiO_2 is an ideal photocatalyst for direct CH_4 conversion because it is very stable with appreciable performance. A core problem of TiO_2 for CH_4 oxidation is that it inclines to deeply oxidize the oxygenated products by generating highly oxidative hydroxyl radical ($^{\bullet}OH$) from photooxidation of water.[28] To develop stable photocatalysts with suppressed overoxidation ability for producing oxygenated products with high selectivity is thus highly desirable.

Herein, we report a dual-cocatalyst, i.e., nanometals (Au, Pd, Ag and Pt) and cobalt oxide (CoO_x) nanoclusters, modified TiO_2 photocatalyst for highly selective room-temperature photocatalytic CH_4 oxidation to CH_3OH with O_2. Upon light irradiation, photoexcited electron separation and O_2 reduction are promoted by nanometals modification. While CoO_x species tunes the nature of oxidative sites of photocatalysts and avoids the direct single electron water oxidation into $^{\bullet}OH$ as occurs over bare TiO_2. Thereby, the overoxidation of CH_3OH to HCHO and CO_2 by highly oxidative $^{\bullet}OH$ can be ultimately suppressed. The highest yield of the primary products, CH_3OOH and CH_3OH reached 2,540 μmol g^{-1} h^{-1} with 95% selectivity over Au-CoO_x/TiO_2, which is outstanding among recently reported low-temperature CH_4 conversion systems.

Experimental section

Synthesis of nanometals/TiO_2. Nanometals (Au, Pt, Ag and Pd) nanoparticles were deposited on TiO_2 (P25) using $NaBH_4$ as reducing reagent. In typical, for synthesis of Au/TiO_2, 1 g TiO_2 and 41.8 mg $HAuCl_4 \cdot 4H_2O$ were dispersed into 50 mL water. After stirring for 2 h, $NaBH_4$ aqueous solution (10 mL, 100 mM) was added into the above mixture. Then, the sample was centrifuged and washed with deionized water for 5 times. The obtained sample was dried overnight at 60 °C. Pt/TiO_2, Pd/TiO_2 and Ag/TiO_2 was synthesized via a similar method except changing the corresponding metal precursors (H_2PtCl_6, Na_2PdCl_4, and $AgNO_3$). The loading amount of Au, Pd, Ag and Pt was estimated to be 1.0 wt.%.

Synthesis of CoO_x/TiO_2. 1 g TiO_2 was mixed with 10 mL a certain amount of $Co(NO_3)_2 \cdot$solution. The slurry was stirred for 6 h and dried at 80 °C. Then, the mixture was annealed at 300 °C with a heating rate of 2 °C min^{-1} for 4 h in air. The obtained samples were denoted as CoO_x/TiO_2. The loading amount of cobalt was calculated assuming the metallic cobalt state. CoO_x/TiO_2 with different Co loading amount were obtained by changing the concentration of $Co(NO_3)_2 \cdot 6H_2O$ aqueous.

Synthesis of nanometals-CoO_x/TiO_2. The method is similar to that of nanometals/TiO_2 but using CoO_x/TiO_2 as the support.

Characterization. TEM, HRTEM and STEM-EDS mapping were conducted on a Tecnai G2 F30 microscope. PXRD was performed on a PANalytical diffractometer with Cu Kα radiation. Inductively coupled plasma atomic emission spectrometry (ICP-AES) was employed to obtain the amount of nanometals and cobalt loaded on the catalyst. Surface chemical states were analyzed

using XPS (PHI Quantera SXMULVAC-PHI, Japan). A USR-40 spectrophotometer was used to measure the wavelength and light intensity of light source. A F-7000 Fluorescence Spectrophotometer (HITACHI) was employed to measure the photoluminescence (PL) spectra using 300 nm excitation wavelength. The PL measurement was performed without the pretreatment of samples. *In-situ* EPR spectroscopy measurements were conducted using a Magnettech MS-5000X instrument. To detect methyl radical, catalyst was dispersed into 5 mL water with CH_4 and O_2 bubbling; to detect hydroperoxyl radicals, catalyst was dispersed into 5 mL CH_3OH/water mixture (9/1 v/v) with O_2 bubbling. 5, 5-Dimethyl-1-pyrroline-*N*-oxide (DMPO) was used as the radical trap. A FT/IR-6300 system (JASCO) with a liguid nitrogen cooled mercury-cadmium-telluride (MCT) detector was used to perform in situ DRIFTS analysis. The reactant gases CH_4/O_2 (20/1, v/v) were introduced into the sample for 20 min before test and then the background was recored under dark condition. After that, the spectra were recorded with UV light irradiation. The photoluminescence technique with coumarin as the fluorescence probe molecule was used to determine the production of hydroxyl radicals.

Photocatalytic methane oxidation evaluation. The photooxidation of CH_4 reactions were performed in a batch-reactor (230 mL). In general, 10 mg catalyst was dispersed into 100 mL water. After introducing oxygen for 20 min to remove air, 0.1 MPa O_2 and 2.0 MPa CH_4 were introduced into the reactor. 300 W Xe lamp (450 mW cm^{-1}, 300-500 nm) was employed as the light source. The reaction temperature at 25±2 °C by utilization of a cold-water bath. After reaction, the reactor was put a refrigerator to reduce the temperature to 8 °C. The reaction gas products were measured by using GC-FID-Methanator. The liquid products (CH_3OOH and CH_3OH) were quantified by ^1H NMR. Briefly, 0.1 mL D_2O and 0.05 μL DMSO (dimethyl sulfoxide, as an internal standard) were mixed with 0.5 mL product solution. The amount of CH_3OOH and CH_3OH were quantified

according to the calibration curves.[27] The amount of formaldehyde was quantified using colorimetric method.[29] Briefly, 2.0 mL colorimetric reagent (0.3 mL acetic acid, 15 g ammonium acetate, 0.2 mL acetylacetone in 100 mL water) was mixed with 0.5 mL product solution. The mixed solution was held 35 °C for around 0.5 h. The absorption intensity of the solution was detected using UV-visible absorption spectroscopy. The amount of HCHO was calculated according to the standard curve.[27]

Computational details. First principle calculations with Vienna Ab initio Simulation package was used to perform all calculations.[30] The projected augmented wave was utilized to generate the pseudopotential. The generalized gradient approximation (GGA) with the Perdew-Burke-Ernzerhfunctional was employed as the exchange-correlation functional.[31] Along the out-plane-direction, we utilized a vacuum layer (16 Å). Co_3O_4 (311) with 164 atoms was used as the model. Its in-plane parameter a is 19.935 Å and b is 11.509 Å. The 1×2×1 k-point mesh-set was utilized for structural relaxing, and the kinetic cut-off energy was set to 400 eV. All structural models were completely relaxed until the convergence of forces and energy were less than 0.01 eV $Å^{-1}$ and 1×10^{-5} eV, respectively.

Results and discussion

In our previous study, we demonstrated that TiO_2 (P25) enabled direct oxidation of CH_4 to HCHO in the presence of O_2 under mild light ($300 < \lambda < 500$ nm, 100 mW cm^{-2}) irradiation in aqueous solution, while no CH_3OOH or CH_3OH was detected by ^1H NMR even by loading 0.1 wt% Au, Pd, Ag and Pt on TiO_2.[27] Considering that HCHO was the product of CH_3OH oxidation, we speculate that TiO_2 is able to photocatalytically oxidize CH_4 to CH_3OH with O_2, and the low CH_3OH concentration in the aqueous solution was probably lower than the limitation of ^1H NMR.

To promote CH_3OH production, the light intensity was increased to 450 mW cm^{-2} and the loading amount of Au, Pd, Ag and Pt was increased to 1.0 wt% (the samples were denoted as Au/TiO_2, Pd/TiO_2, Ag/TiO_2 and Pt/TiO_2) (Table S1). The typical photocatalytic CH_4 oxidation was also carried out in 100 mL water at 25±2 °C for 2 h with 0.1 MPa O_2 and 2 MPa CH_4. Encouragingly, the primary products (CH_3OOH and CH_3OH) was detected by ^1H NMR (Figure S1). As shown in Figure 1a, Pt/TiO_2, Pd/TiO_2 and Au/TiO_2 showed the similar performance for the production of the primary products with the yield of ~ 50 μmol for 2 h reaction. And a higher yield of the primary products (65.8 μmol) was obtained over Ag/TiO_2. Nonetheless, since the primary products underwent facile overoxidation over nanometals/TiO_2, the total amounts of HCHO and CO_2 were higher than those of the primary products, ultimately resulting in low selectivity (< 45%) over all photocatalysts (Figure 1a).

To prevent overoxidation of the desired primary products, cobalt oxide species was loaded on TiO_2 before loading metal cocatalysts (the samples were denoted as Au-CoO_x/TiO_2 Pd- CoO_x/TiO_2, Ag-CoO_x/TiO_2 and Pt-CoO_x/TiO_2). The loading amount of cobalt was 1 wt% (Table S1). Intriguingly, the production of HCHO and CO_2 was remarkably suppressed over nanometals-CoO_x/TiO_2, although the measured yield of the primary products was slightly decreased (Figure 1b). Among these catalysts, Au-CoO_x/TiO_2 showed the lowest production rate of HCHO and CO_2 and the highest selectivity towards the primary products (95 %); the total amounts of HCHO and CO_2 decreased from 88.8 to 2.7 μmol after loading CoO_x, whereas the yield of the primary products only decreased from 53.1 to 50.8 μmol. Ag-CoO_x/TiO_2 showed higher yield of the primary products than Au-CoO_x/TiO_2, yet the selectivity increased only to 71.3%. The apparent quantum efficiency (AQE) of the primary products was determined to be 1.2 % at 368 nm (Table S2). The loading amount of cobalt oxide species has a remarkable effect on the selectivity and activity of

the primary products (Figure S2). The production of the primary products remained almost unchanged and the selectivity continuously increased. with increase of cobalt loading up to 1.0 wt%. The photocatalytic activity declined when loading exceeded 1.0 wt%, probably because the excessive coverage of TiO_2 surface by CoO_x species suppressed the photoexcitation of TiO_2. With increasing irradiation time, the yield of the primary products increased gradually over Au-CoO_x/TiO_2 (Figure S3a). When the irradiation time exceeded 3 h, the yield of the primary products gradually became saturated, while the yields of HCHO and CO_2 gradually increased, and the selectivity towards the primary products thus decreased with irradiation time. A similar trend was observed over Au/TiO_2 (Figure S3b). The CH_4 conversion over Au-CoO_x/TiO_2 is approximately 0.07% and 0.1% at 2 h and 4 h, respectively. While the O_2 conversion is approximately 1.0% and 1.7% at 2 h and 4 h, respectively. The formation rate of the primary products over Au-CoO_x/TiO_2 is higher than most of previously reported photocatalytic CH_4 oxidation to CH_3OH at the similar CH_4 conversion level (Table S3).[27,32-34] In addition, both CH_3OOH and CH_3OH were produced on Au- and Ag-CoO_x/TiO_2, while only CH_3OH was produced on Pt- and Pd-CoO_x/TiO_2. This is probably because Pt and Pd cocatalysts are more active than Au and Ag cocatalysts for the further reduction of CH_3OOH into CH_3OH through a two-electron transfer process ($CH_3OOH + 2e^- + 2H^+ \rightarrow CH_3OH + H_2O$).[27,35]

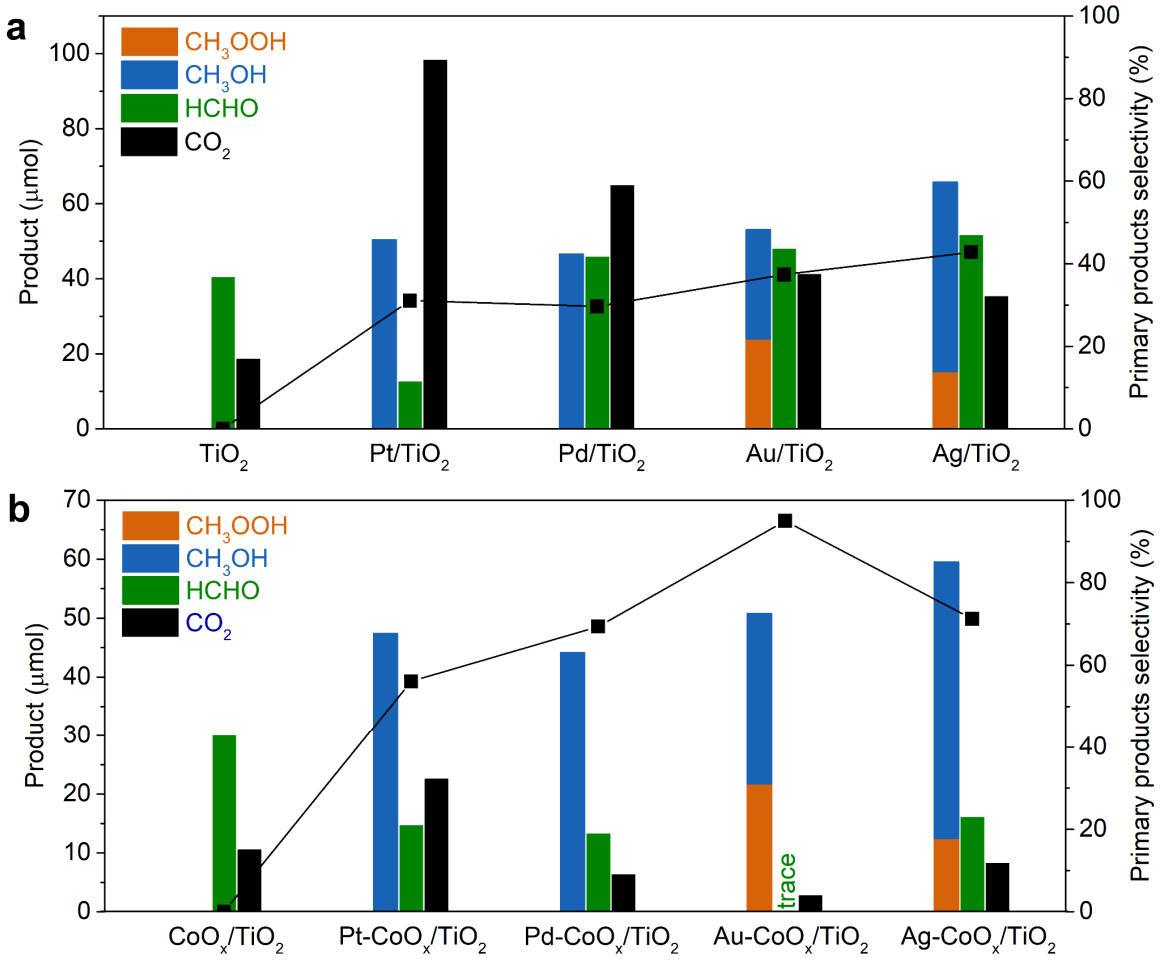

Figure 1. Direct photocatalytic CH_4 oxidation to CH_3OH with O_2. (a) Product yields and primary products selectivity on TiO_2 loaded with or without nanometals after 2 h reaction. (b) Product yields and primary products selectivity on CoO_x/TiO_2 loaded with or without nanometals after 2 h reaction.

Blank experiments without CH_4, light, photocatalysts and O_2 demonstrated that no product was formed (Table S4), revealing that the oxygenates were produced through photocatalytic CH_4 oxidation and O_2 was required to form the primary products. $^{13}CH_4$ isotope experiment was carried out with Au-CoO_x/TiO_2 to demonstrate carbon source in the primaryproducts. Figure 2a shows that two clear peaks appeared at 49 and 65 ppm in the ^{13}C NMR spectrum assigning to CH_3OH and CH_3OOH, respectively, which clearly demonstrates that the formed liquid oxygenates originate from CH_4.[9] Stability is an important issue in catalytic reactions. We investigated the

stability of Au-CoO_x/TiO_2 catalyst in 5 runs under a total of 10 hours of light irradiation (Figure 2b). The catalyst maintained a relatively stable yield and selectivity of the primary products, with only a small decrease. ICP-AES measurement showed no presence of Ti^{4+} in the reaction solution after light irradiation for 2 hours, revealing that no photo-corrosion took place over TiO_2-based catalyst. This result confirms good stability of Au-CoO_x/TiO_2 catalyst. In addition, the turnover number (TON) was calculated to be 2.0 with respect to the amount of TiO_2 after 5 cycling tests.

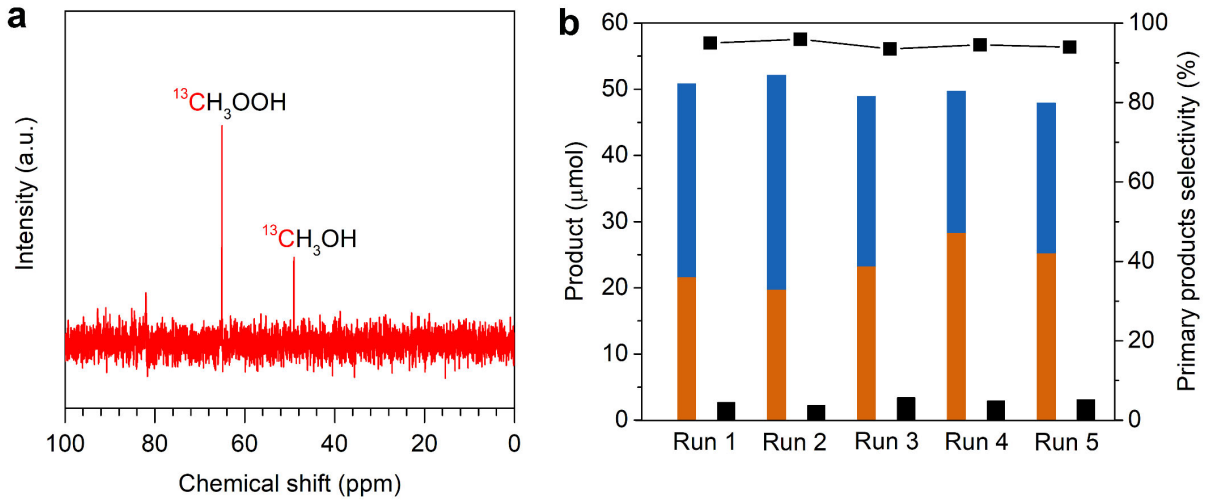

Figure 2. Evidence and stability of photocatalytic CH_4 oxidation to CH_3OH with O_2. (a) ^{13}C NMR spectrum for the reaction solution using 0.4 MPa $^{13}CH_4$ on Au-CoO_x/TiO_2 after 4 h reaction. (b) Stability tests of photocatalytic CH_4 oxidation on Au-CoO_x/TiO_2 in 5 runs with a total of 10 h of light irradiation.

To figure out the activity-structure relationship in photocatalytic CH_4 oxidation by noble metals and cobalt oxide loaded TiO_2, the morphology and structure of these catalysts were investigated. The XRD patterns (Figure S4) shows that all peaks are indexed to TiO_2 and no peak assigned to Pt, Pd, Au, Ag and cobalt oxides are observed, probably because of the small size of loaded noble metals and cobalt oxides. Transmission electron microscopy (TEM) image shows that CoO_x nanoclusters are highly distributed on TiO_2 surface and theirs sizes are approximately 1-2 nm, without obvious aggregation (Figure S5). The size of Au nanoparticles (NPs) dispersed on the

CoO_x/TiO_2 is in the range of 4 to 8 nm (Figure 3a). High-resolution TEM image (Figure 3b) reveals that Au nanoparticles and CoO_x nanoclusters are dispersed on TiO_2 surface. The SAED pattern (Figure S6) shows that two sets of ring patterns indexed to TiO_2 and Au, and no ring pattern attributed to CoO_x nanoclusters, probably due to their amorphous nature.[36] The energy-dispersive X-ray elemental mapping images shows suggested that Au, Co, Ti and O, are uniformly distributed over Au-CoO_x/TiO_2 (Figure 3c and 3d). X-ray photoelectron spectroscopy (XPS) analysis was used to study the chemical states of Au NPs and cobalt oxide species on TiO_2. The Au 4f spectra (Figure 3e) of Au-CoO_x/TiO_2 show two peaks 86.9 and 83.2 eV, revealing the metallic state of Au nanoparticles in Au-CoO_x/TiO_2.[37] Figure 3f shows that two peaks at 781.2 eV and 796.3 eV are atrributed to the Co 2p3/2 and Co 2p1/2, with two satellite peaks of cobalt oxides.[38,39] Compared with the peak at 780.1 eV attributed to Co_3O_4 peaks, the corresponding peak of Au-CoO_x/TiO_2 are shifted to 781.2 eV, implying that the loaded cobalt oxide species are slightly cationic than pure Co_3O_4 and are thus represented as CoO_x.[36] The positive shift of Co 2p peaks agrees well with previous studies and probably results from the strong electronic interaction between CoO_x and TiO_2.[38]

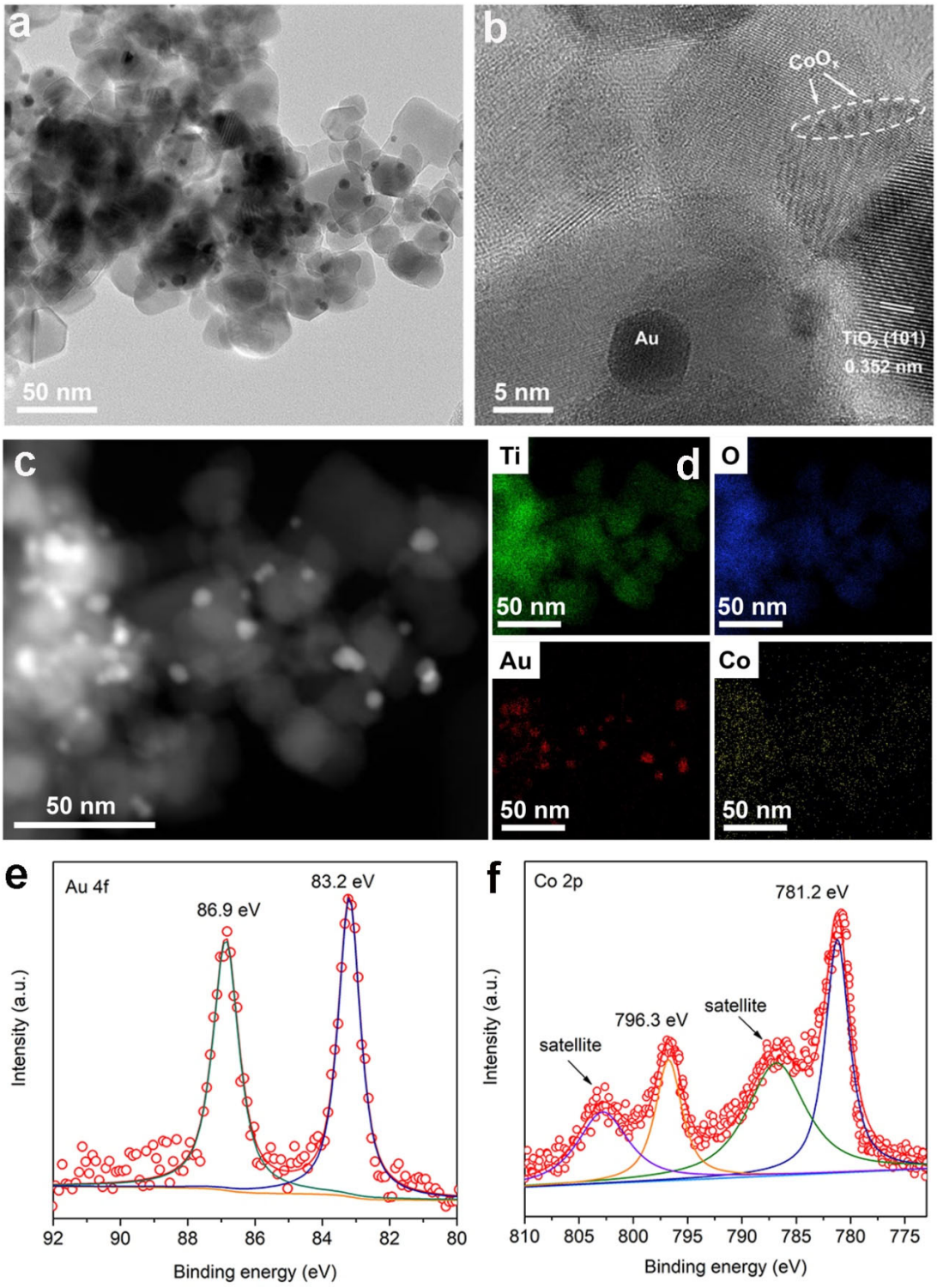

Figure 3. Structure characterization of catalysts. (a) TEM image of Au-CoO_x/TiO_2. (b) High-resolution TEM image of Au-CoO_x/TiO_2. (c) STEM image of Au-CoO_x/TiO_2. (d) Element EDS mapping of Ti, O, Au and Co. (e) Au 4f XPS spectra of Au-CoO_x/TiO_2. (f) Co 2p XPS spectra of Au-CoO_x/TiO_2.

To study the process of photocatalytic CH_4 oxidation with O_2 over Au-CoO_x/TiO_2 catalyst, in-situ electron paramagnetic resonance (EPR) technique was used with DMPO as the radical trap. Figure 4a shows that the signals of $^{\bullet}CH_3$ and $^{\bullet}OH$ radicals are observed under light irradiation.[38] This result suggests that CH_4 oxidation on TiO_2 photocatalyst undergo a radical process with the participation of $^{\bullet}CH_3$.[6,40] The intensities of $^{\bullet}CH_3$ and $^{\bullet}OH$ signals were increased with increasing the illumination time. EPR measurement was performed in methanol aqueous solution dissolving O_2 to measure the intermediate species of O_2 photoreduction.[41] The observed signals are ascribed to radicals, and similarly, increasing the irradiation time could increase the intensity of $^{\bullet}OOH$ signals (Figure 4b). The coulpling reaction between $^{\bullet}CH_3$ and $^{\bullet}OOH$ could take place for the formation of CH_3OOH, which could further decompose to form CH_3OH.[6] Loading CoO_x species slightly decreases the formation of $^{\bullet}CH_3$ and $^{\bullet}OOH$ radicals (Figure S7), consistent with the results of photocatalytic activity.

To further obtain more insights into the details of photocatalytic CH_4 oxidation, in-situ diffuse reflectance infrared fourier transform spectroscopy (DRIFTS) of photocatalysts in the presence of CH_4 and O_2 was carried out. Figure 4c shows time-resolved DRIFT spectra of the oxygenated species of CH_4 photooxidation over Au/TiO_2. Under light irradiation, a peak at 2869 cm^{-1} appears and the corrsponding intensity increases with light illumination. This new band is attributed to the stretching vibration of C-H bond in CH_3OH,[42,43] revealing that CH_3OH is formed in the oxidation process. In addition, the newly emerged bands in the region from 1600-1280 cm^{-1} that can be attributed to the overoxidation products (formate HCOO*, formaldehyde HCOO*, and dioxymethylene CH_2OO* species) also appear,[42,43] the intensity of which grows continuously with increase of irradiation time. Likewise, a substantial increase of the bands of CO_2 at 2361 cm^{-1} and 2330 cm^{-1} is also detected. These results confirm the severe overoxidation of CH_4 over Au/TiO_2

photocatalysts. On the contrary, after loading CoO_x on TiO_2, the intensities of gaseous CO_2 bands and the bands attributed to HCOO*, HCOO*, and CH_2OO* species are much lower over Au-CoO_x/TiO_2 (Figure 4d), indicating that the overoxidation of the CH_3OH produced is suppressed to a large extent. The signals of trace CO_2 is still detected, probably because water was not introduced in the DRIFT measurement. The presence of water in the photocatalytic CH_4 oxidation could assist CH_3OH production and desorption, thus avoiding overoxidation.[44,45]

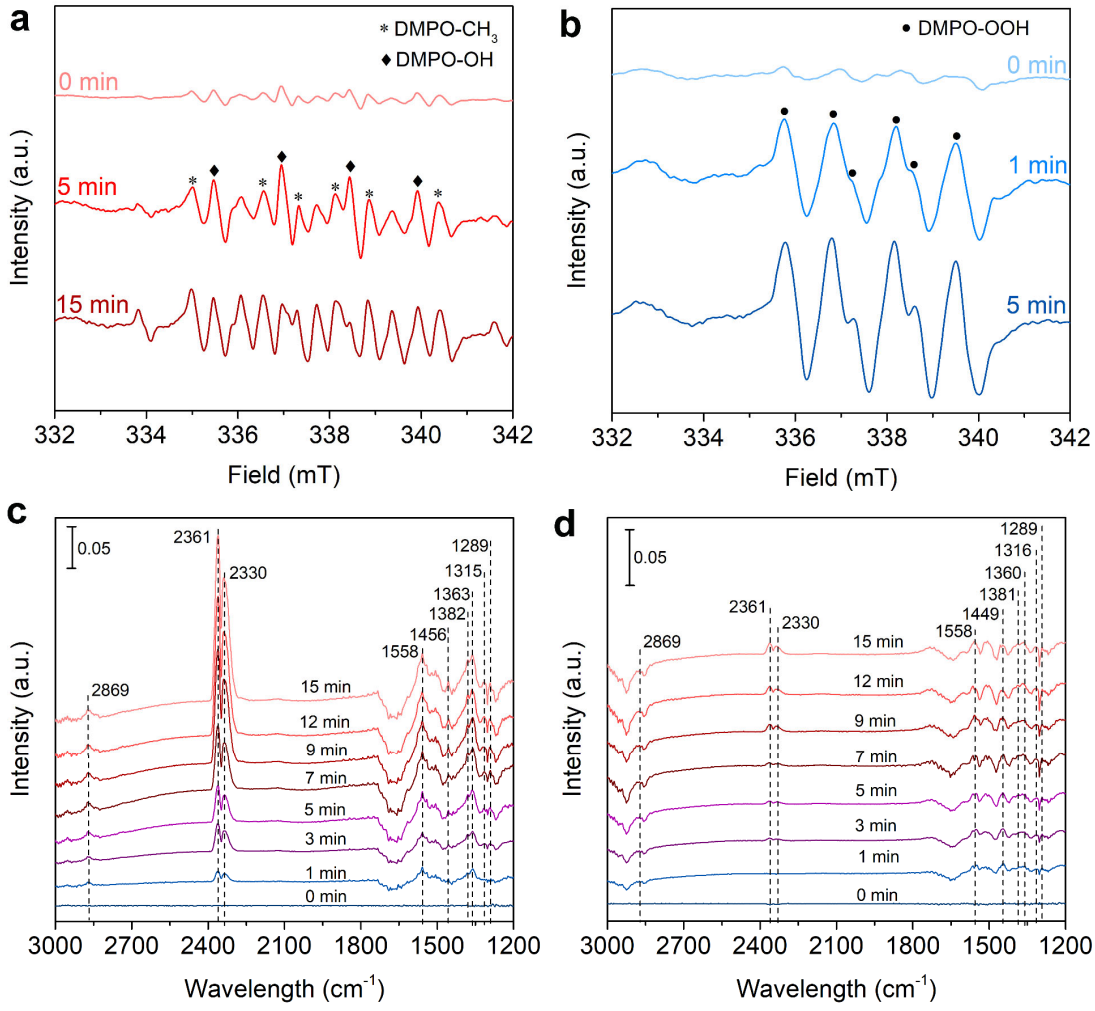

Figure 4. Characterization of intermediate species in photocatalytic CH_4 oxidation. (a) In situ EPR spectra of Au-CoO_x/TiO_2 in water dissolving CH_4 and O_2 with different light illumination time. (b) In situ EPR spectra of Au-CoO_x/TiO_2 in CH_3OH aqueous solution dissolving O_2 with different light illumination time. In situ DRIFT spectra of Au/TiO_2 (c) and Au-CoO_x/TiO_2 (d) under different light irradiation time.

The photoluminescence (PL) spectra of catalysts were studied in order to study the role of CoO_x species and nanometals in photocatalytic CH_4 oxidation. After loading Au NPs and CoO_x species, the PL intensity of TiO_2 decreases remarkably (Figure 5a), suggesting that Au NPs and CoO_x species favorably facilitate photo-induced electron-hole pairs separation. According to the results of photocatalytic activity, loading CoO_x species resultes in the decrease in the production of HCHO and CO_2. We assume that HCHO and CO_2 are originated from photocatalytic CH_3OH oxidation in the presence of O_2. To confirm this, CH_3OH was used as the reactant instead of CH_4. A large amount of HCHO and CO_2 were indeed detected in the products over Au/TiO_2 (Figure S8). Whereas, the amounts of HCHO and CO_2 were significantly decreased over $Au\text{-}CoO_x/TiO_2$ (Figure S8), agreeing well with the photocatalytic performances. It is well known that the photooxidation of CH_3OH to HCHO and CO_2 could be driven by photo-induced holes (h^+) and/or $^{\bullet}OH$ radicals from water.[46] To distinguish which one exert the dominant role in overoxidation of CH_4, experiments using isotopically labeled $^{18}O_2$ or $H_2{}^{18}O$ were conducted. Figure 5b shows the ^{18}O-isotpoe distribution of CO_2 in photocatalytic CH_4 oxidation over $Au\text{-}CoO_x/TiO_2$. When $^{18}O_2$ and $H_2{}^{16}O$ was used, a trace of $C^{16}O^{18}O$ (m/z=46) (5%) was generated, and most of the product was $C^{16}O^{16}O$ (m/z=44) (95%). When the reactants were replaced with $^{16}O_2$ and $H_2{}^{18}O$, the amount of $C^{16}O^{16}O$ (m/z=44), $C^{16}O^{18}O$ (m/z=46) and $C^{18}O^{18}O$ (m/z=48) accounted for 11%, 35% and 54%, respectively. A similar result was obtained over Au/TiO_2 (Figure S9). These results distinctly demonstrate that the oxygen atoms of produced CO_2 are mainly derived from water. Therefore, we can draw the conclusion that $^{\bullet}OH$ radicals from the photooxidation of water has a dominated effect on the formation of CO_2 in photocatalytic CH_4 oxidation. This can be further supported by the experimental results of $^{\bullet}OH$ radicals production over photocatalysts. As shown in Figure 5c, Au, Pd, Ag or Pd -CoO_x/TiO_2 produced much less $^{\bullet}OH$ radicals, as compared to their counterparts Au,

Pd, Ag or Pd-TiO_2, and the low concentration of $^{\bullet}OH$ radicals results in low extent of overoxidation of produced CH_3OH to HCHO and CO_2.

According to the above results, a potential reaction process of selective photooxidation of CH_4 to CH_3OOH and CH_3OH can be proposed (Figure 5d). For nanometals/TiO_2 (taking Au/TiO_2 as an example), upon light irradiation, photo-induced electrons on nanometals can readily reduce O_2 can be readily with proton to produce $^{\bullet}OOH$, and the holes on the surface of TiO_2 can oxidize not only methane to $^{\bullet}CH_3$, and but also water to $^{\bullet}OH$. Isotopic experiments with oxygen demonstrated that the oxygen atoms of formed primary products came from O_2 (Figure S10), consistent with our previously reported work.[27] Thus, $^{\bullet}CH_3$ would interact with $^{\bullet}OOH$ or dissolved O_2 in aqueous reaction solution to form CH_3OOH, which can be further converted to CH_3OH.[6,27] The $^{\bullet}OH$ radicals generated from photo-oxidation of water could further oxidize CH_3OOH and/or CH_3OH to form HCHO and CO_2 (Figure 5d, left), leading to a low selectivity towards the primary products. For CoO_x species modified Au/TiO_2, as the valence band (VB) of Co_3O_4 (~2.4 V_{NHE}) is negative than that of TiO_2 (~3.0 V_{NHE}),[47] a portion of photoexcited holes from TiO_2 would migrate to the surface of CoO_x species, thereby promoting photoinduced holes separation (Figure 5d, right). Because the VB of Co_3O_4 is negative than the potential of $^{\bullet}OH$ production from water ($E^0(^{\bullet}OH/H_2O)$ = 2.8 V_{NHE}),[48] it is unable to oxidize water to produce $^{\bullet}OH$ (Figure 5d, right). The first C-H bond cleavage is regarded as the rate-determining step in CH_4 conversion.[1,2] DFT calculations reveal the barrier of 3.25 eV for first C-H cleavage on Co_3O_4 is (Figure S11), much higher than that on TiO_2 (2.15 eV),[27] revealing that methane is more difficult to be activated on Co_3O_4 than on TiO_2 from a thermodynamic point of view. In addition, CH_4 conversion was reduced after loading CoO_x species (the amounts of the total products were reduced, Figure 1), indicating that loading CoO_x species on TiO_2 seems unfavorable to CH_4 conversion. Both of these two results

confirm that the dissociation of first C-H bond in methane is more likely to be driven by the holes on TiO_2 surface, instead of on CoO_x surface. The holes on CoO_x species are more likely to be consumed for oxygen evolution reaction since CoO_x species is a well-known catalyst for water oxidation in CoO_x/TiO_2 system.[36,49] Isotopic experiment using $H_2{}^{18}O$ as the reactant failed to detect the $^{18}O_2$, probably because only a trace amount of $^{18}O_2$ was produced and the produced $^{18}O_2$ could be further reduced to $H_2{}^{18}O$. The decreased $^{\bullet}OH$ production inhibits the overoxidation of CH_3OOH/CH_3OH by $^{\bullet}OH$ to $HCHO/CO_2$. The lowest formation rate of $^{\bullet}OH$ on $Au\text{-}CoO_x/TiO_2$ results in the highest selectivity towards the primary products (Figure 5c). Au is the best cocatalyst probably due to: it has an appropriate work function to ensure the necessary charge separation[50,51]; it has a mild ability to reduce O_2 to reactive oxygen species (O_2^-, $^{\bullet}OOH$, or $^{\bullet}OH$) to inhibit overoxidation of methanol to HCHO and CO_2. Therefore, in selective photocatalytic CH_4 oxidation, inhibiting the production of $^{\bullet}OH$ in the aqueous medium is an important factor to achieve excellent selectivity for CH_3OH.

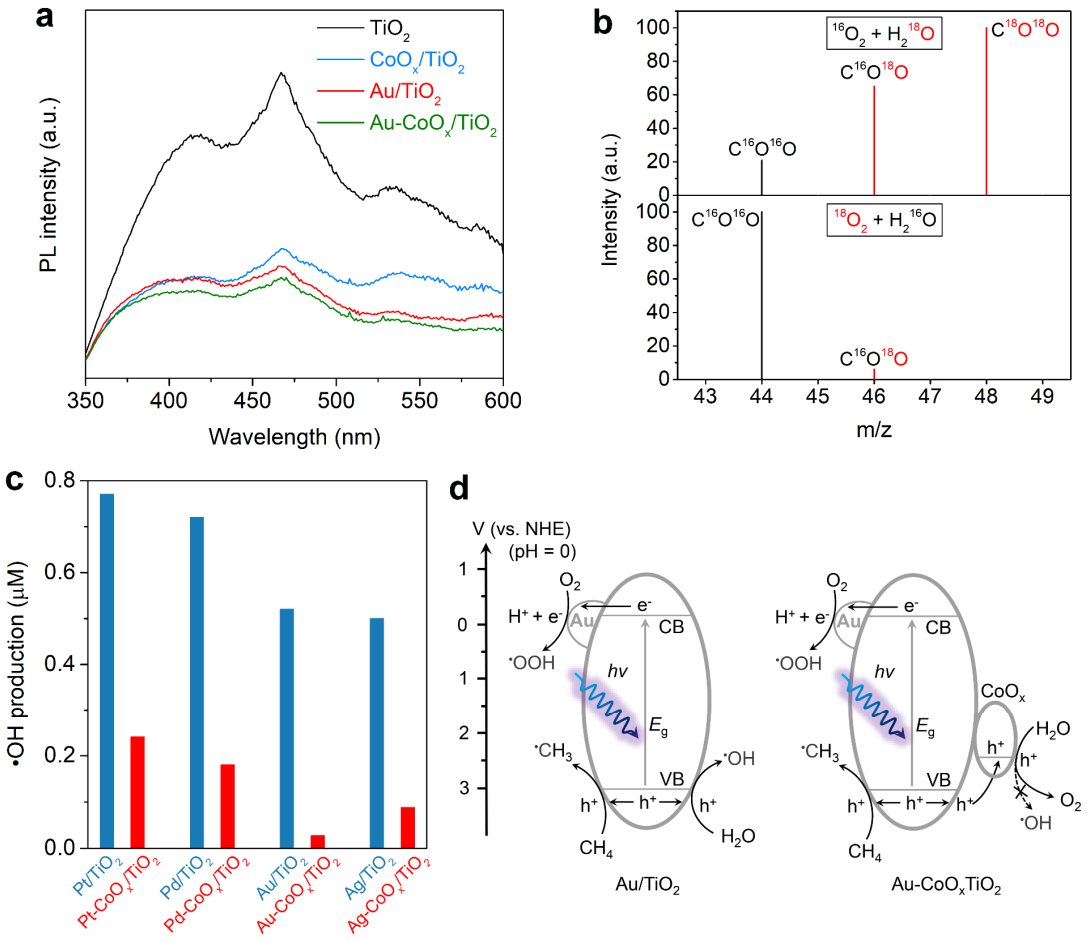

Figure 5. Mechanism of selective photocatalytic CH_4 oxidation to CH_3OH. (a) PL spectra of photocatalysts. (b) GC-MS spectra of CO_2 produced in the presence of $^{16}O_2$ and $H_2{}^{18}O$ or $^{18}O_2$ and $H_2{}^{16}O$ Au-CoO_x/TiO_2. (c) $^{\bullet}OH$ production of photocatalysts in 1 mM coumarin aqueous solution. (d) Proposed reaction process of photocatalytic CH_4 oxidation on Au/TiO_2 and Au-CoO_x/TiO_2 using O_2 as the oxidant.

Conclusions

In conclusion, direct and highly selective photooxidation of CH_4 to CH_3OH with O_2 as the sole oxidant at room temperature was achieved over nanometals and CoO_x modified TiO_2 photocatalysts. Nanometals cocatalysts facilitated the production of oxygenated products, and CoO_x species suppress the formation of highly oxidative $^{\bullet}OH$ radicals production, which efficiently prevented the overoxidation of CH_3OH to HCHO and CO_2. The synergistic effect of

nanometals and CoO_x nanoclusters resulted in high activity and selectivity for methanol production. Up to 50.8 μmol of the primary products for 2 h with 95% selectivity was achieved over 10 mg of optimized Au-CoO_x/TiO_2 catalyst. This work offers an approach to direct and selective photocatalytic oxidation of CH_4 to CH_3OH with O_2.

ASSOCIATED CONTENT

Supporting Information

The Supporting Information is available free of charge on the ACS Publications website.

Additional experimental data and results including physicochemical properties of catalysts, ^{1}H NMR spectrum, AQE calculation, photocatalytic activity, comparison of catalytic activity in methane oxidation methanol, TEM image, SAED pattern, EPR spectra, GC-MS spectra and DFT calculations.

AUTHOR INFORMATION

Corresponding Authors

Email: Jinhua.YE@nims.go.jp;

mengxg_materchem@163.com;

wangshengyao@mail.hzau.edu.cn

Notes

The authors declare no competing financial interests.

ACKNOWLEDGMENT

This work received the financial support from Photo-excitonix Project in Hokkaido University, JSPS KAKENHI Grant Number JP18H02065, National Natural Science Foundation of China

(No. 21633004 and No.51872091) and Hundred Talents Program of Hebei Province (E2018050013).

REFERENCES

(1) Ravi, M.; Ranocchiari, M.; van Bokhoven, J. A. The direct catalytic oxidation of methane to methanol-A critical assessment. *Angew. Chem. Int. Ed.* **2017**, *56*, 16464-16483.

(2) Schwach, P.; Pan, X.; Bao, X. Direct Conversion of Methane to Value-Added Chemicals over Heterogeneous Catalysts: Challenges and Prospects. *Chem. Rev.* **2017**, *117*, 8497-8520.

(3) Olivos-Suarez, A. I.; Szécsényi, À.; Hensen, E. J. M.; Ruiz-Martinez, J.; Pidko, E. A.; Gascon, J. Strategies for the Direct Catalytic Valorization of Methane Using Heterogeneous Catalysis: Challenges and Opportunities. *ACS Catal.* **2016**, *6*, 2965-2981.

(4) Tang, P.; Zhu, Q.; Wu, Z.; Ma, D. Methane activation: the past and future. *Energ Environ. Sci.* **2014**, *7*, 2580-2591.

(5) Ravi, M.; Sushkevich, V. L.; Knorpp, A. J.; Newton, M. A.; Palagin, D.; Pinar, A. B.; Ranocchiari, M.; Van Bokhoven, J. A. Misconceptions and challenges in methane-to-methanol over transition-metal-exchanged zeolites. *Nat. Catal.* **2019**, *1*, 485-494.

(6) Agarwal, N.; Freakley, S. J.; McVicker, R. U.; Althahban, S. M.; Dimitratos, N.; He, Q.; Morgan, D. J.; Jenkins, R. L.; Willock, D. J.; Taylor, S. H. Aqueous Au-Pd colloids catalyze selective CH4 oxidation to CH_3OH with O_2 under mild conditions. *Science* **2017**, *358*, 223-227.

(7) Ceri, H.; M., F. M.; Hasbi, A. R. M.; Adam, T.; Qian, H.; L., J. R.; Nikolaos, D.; A., L.-S. J.; F., D. N.; M., M. D.; F., C. A.; H., T. S.; J., W. D.; E., S. E.; Joo, K.; Henk, H.; J., K. C.; J., H. G. Direct Catalytic Conversion of Methane to Methanol in an Aqueous Medium by using Copper-Promoted Fe-ZSM-5. *Angew. Chem. Int. Ed.* **2012**, *51*, 5129-5133.

(8) Sushkevich, V. L.; Palagin, D.; Ranocchiari, M.; van Bokhoven, J. A. Selective anaerobic oxidation of methane enables direct synthesis of methanol. *Science* **2017**, *356*, 523-527.

(9) Cui, X.; Li, H.; Wang, Y.; Hu, Y.; Hua, L.; Li, H.; Han, X.; Liu, Q.; Yang, F.; He, L. Room-temperature methane conversion by graphene-confined single iron atoms. *Chem* **2018**, *4*, 1902-1910.

(10) Kwon, Y.; Kim, T. Y.; Kwon, G.; Yi, J.; Lee, H. Selective Activation of Methane on Single-Atom Catalyst of Rhodium Dispersed on Zirconia for Direct Conversion. *J. Am. Chem. Soc.* **2017**, *139*, 17694-17699.

(11) Shan, J.; Li, M.; Allard, L. F.; Lee, S.; Flytzani-Stephanopoulos, M. Mild oxidation of methane to methanol or acetic acid on supported isolated rhodium catalysts. *Nature* **2017**, *551*, 605-608.

(12) Wang, S.; Hai, X.; Ding, X.; Chang, K.; Xiang, Y.; Meng, X.; Yang, Z.; Chen, H.; Ye, J. Light-Switchable Oxygen Vacancies in Ultrafine Bi_5O_7Br Nanotubes for Boosting Solar-Driven Nitrogen Fixation in Pure Water. *Adv. Mater.* **2017**, *29*, 1701774.

(13) Meng, X.; Zuo, G.; Zong, P.; Pang, H.; Ren, J.; Zeng, X.; Liu, S.; Shen, Y.; Zhou, W.; Ye, J. A rapidly room-temperature-synthesized Cd/ZnS: Cu nanocrystal photocatalyst for highly efficient solar-light-powered CO_2 reduction. *Appl.Catal. B* **2018**, *237*, 68-73.

(14) Tong, H.; Ouyang, S.; Bi, Y.; Umezawa, N.; Oshikiri, M.; Ye, J. Nano-photocatalytic materials: possibilities and challenges. *Adv. Mater.* **2012**, *24*, 229-251.

(15) Wang, Z.; Song, H.; Liu, H.; Ye, J. Coupling of Solar Energy and Thermal Energy for Carbon Dioxide Reduction: Status and Prospects. *Angew. Chem. Int. Ed.* **2020**, *59*, 8016-8035.

(16) Liu, G.; Wang, T.; Zhang, H.; Meng, X.; Hao, D.; Chang, K.; Li, P.; Kako, T.; Ye, J. Nature-Inspired Environmental "Phosphorylation" Boosts Photocatalytic H_2 Production over Carbon Nitride Nanosheets under Visible-Light Irradiation. *Angew. Chem. Int. Ed.* **2015**, *54*, 13561-13565.

(17) Song, H.; Meng, X.; Wang, Z.-j.; Liu, H.; Ye, J. Solar-Energy-Mediated Methane Conversion. *Joule* **2019**, *3*, 1606-1636.

(18) Yuliati, L.; Yoshida, H. Photocatalytic conversion of methane. *Chem. Soc. Rev.* **2008**, *37*, 1592-1602.

(19) Li, Z.; Pan, X.; Yi, Z. Photocatalytic oxidation of methane over CuO-decorated ZnO nanocatalysts. *J. Mater. Chem. A* **2019**, *7*, 469-475.

(20) Chen, X.; Li, Y.; Pan, X.; Cortie, D.; Huang, X.; Yi, Z. Photocatalytic oxidation of methane over silver decorated zinc oxide nanocatalysts. *Nat. Commun.* **2016**, *7*, 12273.

(21) Yu, X.; De Waele, V.; Löfberg, A.; Ordomsky, V.; Khodakov, A. Y. Selective photocatalytic conversion of methane into carbon monoxide over zinc-heteropolyacid-titania nanocomposites. *Nat. Commun.* **2019**, *10*, 700.

(22) Shimura, K.; Kawai, H.; Yoshida, T.; Yoshida, H. Bifunctional rhodium cocatalysts for photocatalytic steam reforming of methane over alkaline titanate. *ACS Catal.* **2012**, *2*, 2126-2134.

(23) Murcia-López, S.; Villa, K.; Andreu, T.; Morante, J. R. Partial Oxidation of Methane to Methanol Using Bismuth-Based Photocatalysts. *ACS Catal.* **2014**, *4*, 3013-3019.

(24) Yu, X.; Zholobenko, V. L.; Moldovan, S.; Hu, D.; Wu, D.; Ordomsky, V. V.; Khodakov, A. Y. Stoichiometric methane conversion to ethane using photochemical looping at ambient temperature. *Nat. Energy* **2020**, 1-9.

(25) Xie, J.; Jin, R.; Li, A.; Bi, Y.; Ruan, Q.; Deng, Y.; Zhang, Y.; Yao, S.; Sankar, G.; Ma, D. Highly selective oxidation of methane to methanol at ambient conditions by titanium dioxide-supported iron species. *Nat. Catal.* **2018**, *1*, 889-896.

(26) Dinh, K. T.; Sullivan, M. M.; Serna, P.; Meyer, R. J.; Dincă, M.; Román-Leshkov, Y. Viewpoint on the Partial Oxidation of Methane to Methanol Using Cu- and Fe-Exchanged Zeolites. *ACS Catal.* **2018**, *8*, 8306-8313.

(27) Song, H.; Meng, X.; Wang, S.; Zhou, W.; Wang, X.; Kako, T.; Ye, J. Direct and Selective Photocatalytic Oxidation of CH_4 to Oxygenates with O_2 on Cocatalysts/ZnO at Room Temperature in Water. *J. Am. Chem.Soc.* **2019**, *141*, 20507-20515.

(28) Hoffmann, M. R.; Martin, S. T.; Choi, W.; Bahnemann, D. W. Environmental applications of semiconductor photocatalysis. *Chem. Rev.* **1995**, *95*, 69-96.

(29) Chen, J.; Stepanovic, S.; Draksharapu, A.; Gruden, M.; Browne, W. R. Non-Heme Iron Photocatalyst for Light-Driven Aerobic Oxidation of Methanol. *Angew. Chem. Int. Ed.* **2018**, *57* (12), 3207-3211.

(30) Kresse, G.; Furthmüller, J.; Efficiency of ab-initio total energy calculations for metals and semiconductors using a plane-wave basis set. *Comput. Mater. Sci.* **1996**, *6*, 15-50.

(31) Perdew, J. P.; Burke, K.; Ernzerhof, M.; Generalized gradient approximation made simple. *Phy. Rev. Lett.* **1996,***77*, 3865.

(32) Murcia-López, S.; Villa, K.; Andreu, T.; Morante, J. R.; Partial Oxidation of Methane to Methanol Using Bismuth-Based Photocatalysts. *ACS Catal.* **2014**, *4*, 3013-3019.

(33) Villa, K.; Murcia-López, S.; Andreu, T.; Morante, J. R.; Mesoporous WO_3 photocatalyst for the partial oxidation of methane to methanol using electron scavengers. *Appl.Catal. B* **2015**, *163* 150-155.

(34) Villa, K.; Murcia-López, S.; Morante, J. R.; Andreu, T. An insight on the role of La in mesoporous WO_3 for the photocatalytic conversion of methane into methanol. *Appl.Catal. B* **2016**, *187*, 30-36.

(35) Siahrostami, S.; Verdaguer-Casadevall, A.; Karamad, M.; Deiana, D.; Malacrida, P.; Wickman, B.; Escudero-Escribano, M.; Paoli, E. A.; Frydendal, R.; Hansen, T. W. Enabling direct H_2O_2 production through rational electrocatalyst design. *Nat. Mater.* **2013**, *12*, 1137-1143.

(36) Maeda, K.; Ishimaki, K.; Okazaki, M.; Kanazawa, T.; Lu, D.; Nozawa, S.; Kato, H.; Kakihana, M. Cobalt oxide nanoclusters on rutile titania as bifunctional units for water oxidation catalysis and visible light absorption: understanding the structure–activity relationship. *ACS Appl. Mater. Interfaces* **2017**, *9*, 6114-6122.

(37) Li, H.; Qin, F.; Yang, Z.; Cui, X.; Wang, J.; Zhang, L. New reaction pathway induced by plasmon for selective benzyl alcohol oxidation on BiOCl possessing oxygen vacancies. *J. Am. Chem.Soc.* **2017**, *139*, 3513-3521.

(38) Ma, T. Y.; Dai, S.; Jaroniec, M.; Qiao, S. Z. Metal-organic framework derived hybrid Co3O4-carbon porous nanowire arrays as reversible oxygen evolution electrodes. *J. Am. Chem.Soc.* **2014**, *136*, 13925-13931.

(39) Wu, W.; Zhang, Q.; Wang, X.; Han, C.; Shao, X.; Wang, Y.; Liu, J.; Li, Z.; Lu, X.; Wu, M. Enhancing selective photooxidation through Co–Nx-doped carbon materials as singlet oxygen photosensitizers. *ACS Catal.* **2017**, *7*, 7267-7273.

(40) Ab Rahim, M. H.; Forde, M. M.; Jenkins, R. L.; Hammond, C.; He, Q.; Dimitratos, N.; Lopez-Sanchez, J. A.; Carley, A. F.; Taylor, S. H.; Willock, D. J.; Murphy, D. M.; Kiely, C. J.; Hutchings, G. J. Oxidation of methane to methanol with hydrogen peroxide using supported gold-palladium alloy nanoparticles. *Angew. Chem. Int. Ed.* **2013**, *52*, 1280-1284.

(41) Chen, C.; Lei, P.; Ji, H.; Ma, W.; Zhao, J.; Hidaka, H.; Serpone, N. Photocatalysis by titanium dioxide and polyoxometalate/TiO_2 cocatalysts. Intermediates and mechanistic study. *Environ. Sci. Technol.* **2004**, *38*, 329-337.

(42) Chen, T.; Feng, Z.; Wu, G.; Shi, J.; Ma, G.; Ying, P.; Li, C. Mechanistic studies of photocatalytic reaction of methanol for hydrogen production on Pt/TiO_2 by in situ Fourier transform IR and time-resolved IR spectroscopy. *J. Phys. Chem. C* **2007**, *111*, 8005-8014.

(43) Nomikos, G. N.; Panagiotopoulou, P.; Kondarides, D. I.; Verykios, X. E. Kinetic and mechanistic study of the photocatalytic reforming of methanol over Pt/TiO_2 catalyst. *Appl.Catal. B* **2014**, *146*, 249-257.

(44) Lustemberg, P. G.; Palomino, R. M.; Gutierrez, R. A.; Grinter, D. C.; Vorokhta, M.; Liu, Z.; Ramirez, P. J.; Matolin, V.; Ganduglia-Pirovano, M. V.; Senanayake, S. D.; Rodriguez, J. A. Direct Conversion of Methane to Methanol on Ni-Ceria Surfaces: Metal-Support Interactions and Water-Enabled Catalytic Conversion by Site Blocking. *J. Am. Chem. Soc.* **2018**, *140*, 7681-7687.

(45) Liu, Z.; Huang, E.; Orozco, I.; Liao, W.; Palomino, R. M.; Rui, N.; Duchoň, T.; Nemšák, S.; Grinter, D. C.; Mahapatra, M. Water-promoted interfacial pathways in methane oxidation to methanol on a CeO_2-Cu_2O catalyst. *Science* **2020**, *368*, 513-517.

(46) Wang, C.-y.; Pagel, R.; Bahnemann, D. W.; Dohrmann, J. K. Quantum yield of formaldehyde formation in the presence of colloidal TiO_2-based photocatalysts: effect of intermittent illumination, platinization, and deoxygenation. *J. Phys. Chem. B* **2004**, *108*, 14082-14092.

(47) Wang, P.; Zheng, J. Y.; Zhang, D.; Kang, Y. S. Selective construction of junctions on different facets of $BiVO_4$ for enhancing photo-activity. *New J. Chem.* **2015**, *39*, 9918-9925.

(48) Lee, H.; Kim, H.-i.; Weon, S.; Choi, W.; Hwang, Y. S.; Seo, J.; Lee, C.; Kim, J.-H. Activation of persulfates by graphitized nanodiamonds for removal of organic compounds. *Environ. Sci. Technol.* **2016**, *50*, 10134-10142.

(49) Maeda, K.; Ishimaki, K.; Tokunaga, Y.; Lu, D.; Eguchi, M. Modification of wide-band-gap oxide semiconductors with cobalt hydroxide nanoclusters for visible-light water oxidation. *Angew. Chem. Int. Ed.* **2016**, *55*, 8309-8313.

(50) Yuzawa, H.; Mori, T.; Hideaki, I.; Yoshida, H. Reaction Mechanism of Ammonia Decomposition to Nitrogen and Hydrogen over Metal Loaded Titanium Oxide Photocatalyst. *J. Phys. Chem. C* **2012***, 116,* 4126 -4136.

(51) Michaelson B. H. The work function of the elements and tis periodicity. *J. Appl. Phys.* **1977**, *48*, 4729-4733.

Table of Contents graphic